



CHORUS

This is the accepted manuscript made available via CHORUS. The article has been published as:

Field-induced double dome and Bose-Einstein condensation in the crossing quantum spin chain system AgVOAsO_4

Franziska Weickert, Adam A. Aczel, Matthew B. Stone, V. Ovidiu Garlea, Chao Dong, Yoshimitsu Kohama, Roman Movshovich, Albin Demuer, Neil Harrison, Monika B. Gamza, Alexander Steppke, Manuel Brando, Helge Rosner, and Alexander A. Tsirlin

Phys. Rev. B **100**, 104422 — Published 17 September 2019

DOI: [10.1103/PhysRevB.100.104422](https://doi.org/10.1103/PhysRevB.100.104422)

Field-induced double phase and Bose-Einstein condensation in the crossing quantum spin chain system AgVOAsO_4

Franziska Weickert,^{1,*} Adam A. Aczel,^{2,†} Matthew B. Stone,² V. Ovidiu Garlea,² Chao Dong,³ Yoshimitsu Kohama,³ Roman Movshovich,⁴ Albin Demuer,⁵ Neil Harrison,⁶ Monika B. Gamza,^{7,8} Alexander Steppke,⁷ Manuel Brando,⁷ Helge Rosner,⁷ and Alexander A. Tsirlin^{7,9}

¹*NHMFL, Florida State University, Tallahassee, FL 32310, USA*

²*Neutron Scattering Division, Oak Ridge National Laboratory, Oak Ridge, TN 37831, USA*

³*ISSP, International MegaGauss Science Laboratory,*

University of Tokyo, Kashiwa Chiba 277-8581, Japan

⁴*MPA-CMMS, Los Alamos National Laboratory, Los Alamos, NM 87545 USA*

⁵*GHMFL, CNRS, 38042 Grenoble cedex 9, France*

⁶*MPA-Mag, Los Alamos National Laboratory, Los Alamos, NM 87545, USA*

⁷*MPI CPfS, Nöthnitzer Str. 40, 01187 Dresden, Germany*

⁸*Jeremiah Horrocks Institute for Mathematics, Physics, and Astrophysics,*

University of Central Lancashire, Preston PR1 2HE, UK

⁹*Experimental Physics VI, Augsburg University, 86135 Augsburg, Germany*

(Dated: June 7, 2019)

Abstract

We present inelastic neutron scattering data on the quantum paramagnet AgVOAsO_4 that establish this system as a $S = 1/2$ alternating spin chain compound and provide a direct measurement of the spin gap $\Delta = 1.2$ meV. We also present experimental evidence for two different types of field-induced magnetic order between $\mu_0 H_{c1} = 8.4$ T and $\mu_0 H_{c2} = 48.9$ T, which may be related to Bose-Einstein condensation (BEC) of triplons. Thermodynamic measurements in magnetic fields up to 60 T and temperatures down to 0.1 K reveal a $H - T$ phase diagram consisting of a dome encapsulating two ordered phases with maximum ordering temperatures of 3.8 K and 5.3 K respectively. This complex phase diagram is not expected for a single- \vec{Q} BEC system and therefore establishes AgVOAsO_4 as a promising multi- \vec{Q} BEC candidate capable of hosting exotic vortex phases.

I. INTRODUCTION

Magnetic vortices are topological objects expected by theory¹ to occur in quantum magnets with spin gapped ground states and field-induced XY-antiferromagnetic (AFM) order with a z -axis spin modulation that can be described within the formalism of Bose-Einstein condensation (BEC). Their close similarity to magnetic skyrmions make them highly attractive for technological applications, because skyrmions i.e. are discussed as energetically robust basic units for memory storage. Whereas magnetic skyrmions have been observed experimentally in metallic MnSi² and insulating Cu₂OSeO₃³ gathering significant scientific attention in recent years, the observation of magnetic vortices in quantum paramagnets has been elusive so far. A necessary condition for the observation of magnetic vortices is the emergence of a multi- \vec{Q} BEC. Here, linear combinations of multiple ordering vectors \vec{Q} can lead to incommensurate AFM order in adjacent phases under the application of a magnetic field, in contrast to single- \vec{Q} BEC, where only one commensurate XY-AFM phase is observed.

Single- \vec{Q} BEC materials often consist of interacting $S = 1/2$ spin dimers and the non-magnetic $S = 0$ singlet ground state is separated from the excited $S = 1$ triplet states by a spin gap, Δ , with a finite dispersion for the triplet excitation arising from the interdimer exchange interactions⁴⁻¹³. An applied magnetic field, H , splits the triplet into its three branches according to their S^z quantum number. As the magnetic field increases, the spin gap closes at a critical field, H_{c1} , and generates field-induced magnetic order. If $O(2)$ rotational invariance is preserved above H_{c1} , then this ordered state is equivalent to a BEC of $S^z = 1$ triplons¹⁴⁻¹⁸. At higher fields, a saturated magnetic phase is generated above H_{c2} . The main difference between single- \vec{Q} and multi- \vec{Q} BEC materials are competing interdimer exchange interactions only present in the latter case. Frustration modifies the triplet dispersion of a multi- \vec{Q} BEC material in a way that several degenerate minima occur inside a single Brillouin zone (BZ), whereas only one exists at the BZ border in the single- \vec{Q} case.

One promising material recently discussed in the context of multi- \vec{Q} BEC is Ba₃Mn₂O₈. Inelastic neutron scattering (INS) measurements^{19,20} report evidence for frustrated interdimer exchange and a triplet dispersion consisting of several energy minima in a single Brillouin zone. Intriguingly, thermodynamic and torque magnetometry measurements de-

terminated that the H - T phase diagram was more complex than expected for a single- \vec{Q} BEC system, with two ordered phases I and II found for all field orientations except $\vec{H} \parallel c$ where only one ordered phase was uncovered^{9,21}. Subsequent neutron diffraction measurements in a horizontal scattering plane with an applied field $\vec{H} \parallel a^*$ identified phases I and II as an incommensurate spin spiral and spin density wave state respectively²², but nuclear magnetic resonance (NMR) work argued that the BEC description only holds for $\vec{H} \parallel c$ ²³. Other material candidates are therefore required, if one hopes to identify exotic multi- \vec{Q} BEC states, including the magnetic vortex crystal, in the laboratory.

To this end, we propose AgVOAsO₄ as a $S = 1/2$ compound to be a promising multi- \vec{Q} BEC candidate. Vanadium V⁴⁺ is a magnetically isotropic ion with small spin-orbit coupling favoring magnetic ordered ground states of high symmetry as represented by BEC. The monoclinic crystal structure of AgVOAsO₄ consists of corner-sharing VO₆ octahedra that form structural chains along the crystallographic c -direction; these chains are linked to one another via AsO₄ tetrahedra to form a three-dimensional network. The crystal structure is shown in Fig.1 with (a) illustrating the crystal structure viewed roughly along the c -axis. There are chain structures along this axis with a V-V distance of 3.639Å at T = 20 K. In Fig.1 (b) we reproduce the proposed spin model²⁴ showing only the V sites. We note that the J_a and J_c exchange connect spins between layers. In Figures 1(c) and (d) we show views along the (110) and (1 $\bar{1}$ 0) direction. There are two types of structural chains along these directions, which are arranged nearly orthogonal to each other. We label these two chains as type-i and type-ii. The two chains have very similar vectors and distances between V sites, but their bonding is quite different. The type-i chain structure has a much more planar configuration of coordinated oxygen atoms than the type-ii chain as shown in the middle layer of chains in Fig.1(c). When viewed along the (1 $\bar{1}$ 0) direction, it is the top and bottom layers of chains (Fig.1(d)) that have a more planar oxygen coordination. The type-i chain, shown in Fig.1(e) has been considered to be the magnetic alternating chain based upon DFT calculations²⁴ with d_i being the dimer-bond, J , whereas d'_i is the distance of the inter-dimer interaction, J' . The dimer-dimer vector is $u_0 = d_i + d'_i$, which corresponds to the (110) and (1 $\bar{1}$ 0) directions depending upon which ab-plane the chain resides within. The V-V vectors at 20K are $d_i = [0.488, -0.525, 0.060]$ and $[0.488, 0.525, 0.060]$ ($|d_i| = 5.59\text{Å}$), $d'_i = [0.512, -0.475, -0.060]$ and $[0.512, 0.475, -0.060]$ ($|d'_i| = 5.56\text{Å}$), $d_{ii} = [0.512, 0.525, -0.060]$ and $[-0.512, 0.525, 0.060]$ ($|d'_{ii}| = 5.90\text{Å}$), $d_{ii} = [0.488, 0.475, 0.060]$ and $[-0.488, 0.475,$

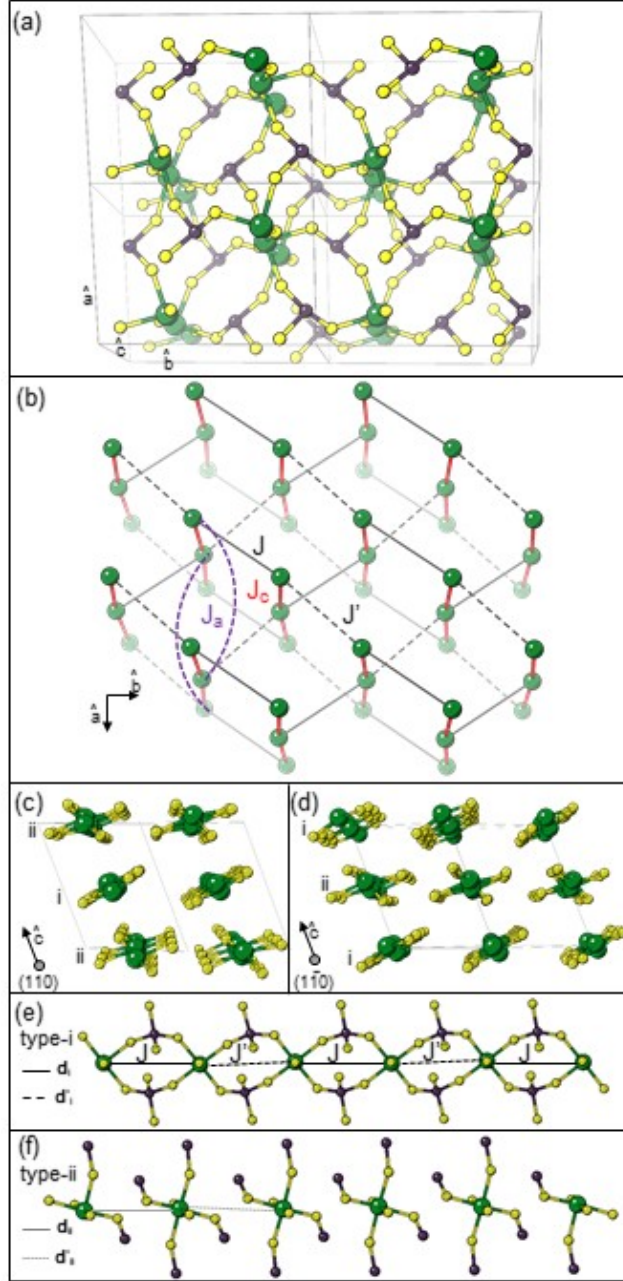


FIG. 1. Crystal structure of AgVOAsO₄. V atoms are large green spheres, O atoms are small yellow spheres and As atoms are black spheres. The Ag atoms are not shown for clarity. (a) Crystal structure viewed obliquely along the c -axis. (b) Exchange paths viewed roughly along the c -axis. For clarity, the J_a interaction is shown only for a single ac -plane and only the V sites are shown. (c) The crystal structure viewed along the (110) direction. (d) The crystal structure viewed along the $(1\bar{1}0)$ direction. In (c) and (d), chains of type-i and type-ii are labeled accordingly. (e) Type-i structural chain with exchange interactions J and J' labeled for vectors d_i and d'_i respectively. (f) Type-ii structural chain with vectors d_{ii} and d'_{ii} shown.

-0.060] ($|d'_{ii}| = 5.23\text{\AA}$).

Bulk characterization and ^{75}As NMR measurements suggest that AgVOAsO_4 is a quantum paramagnet based on alternating spin chains^{25,26} with a spin gap $\Delta = 1.1$ meV, $\mu_0 H_{c1} = 10$ T, a saturation field $\mu_0 H_{c2} = 48.5$ T, and an intrachain exchange ratio $\alpha = J'/J \simeq 0.6\text{-}0.7$ ^{24,27}. DFT calculations furthermore predict significant, competing interchain exchange interactions leading to a large degree of magnetic frustration, which may produce the complicated triplet dispersion that is a prerequisite for a multi- \vec{Q} BEC. The relatively small spin gap ensures that these field-induced ordered states are accessible in the laboratory. In this work, we first show INS results on polycrystalline AgVOAsO_4 that establish the alternating spin chain model²⁴ and provide a direct measurement of the spin gap. Second, we present a comprehensive study of the field-induced magnetic order in this material. Our combined specific heat, magnetization, and magnetocaloric effect (MCE) measurements on polycrystalline samples establish a complex $H - T$ phase diagram with two different field-induced ordered states, which is not expected for a single- \vec{Q} BEC system. Therefore, AgVOAsO_4 is a strong candidate for hosting multi- \vec{Q} BEC.

II. EXPERIMENTAL RESULTS

A. Neutron scattering experiments

The synthesis of polycrystalline samples is described elsewhere²⁴. INS data were collected on 10g of AgVOAsO_4 using the HYSPEC spectrometer of the Spallation Neutron Source, Oak Ridge National Lab (ORNL). All data were obtained using incident energies of $E_i = 7.5$ or 15 meV, with corresponding Fermi chopper frequencies of 180 and 300 Hz, resulting in instrumental energy resolutions of 0.3 and 0.7 meV Gaussian full-width half-maximum respectively at the elastic line. The HYSPEC instrument is able to extend the range of measured wavevector transfer, Q , at a fixed incident energy by moving its detector bank to larger scattering angles. This was done for both the $E_i = 7.5$ and 15 meV measurements presented here. A liquid He cryostat was used during the measurements to achieve temperatures between 3.2 and 200 K.

Fig. 2(a) and (b) show INS data collected at the HYSPEC instrument with energy resolution $E_i = 7.5$ meV at $T = 50$ and 3.2 K, respectively. At 3.2K, we observe a band of

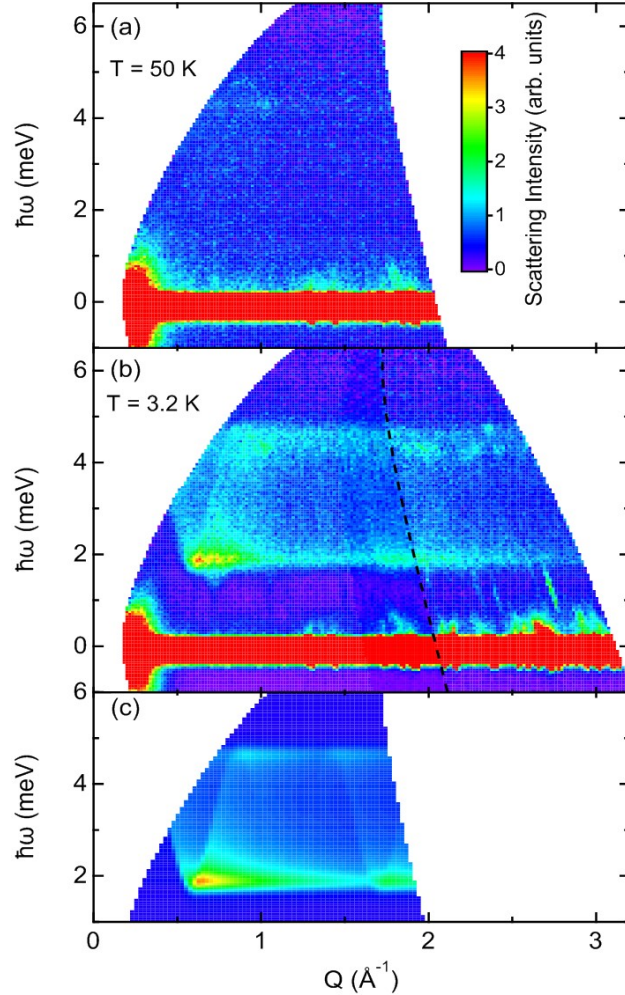


FIG. 2. (a), (b) Color contour plots of the $E_i = 7.5$ meV HYSPEC data for AgVOAsO_4 at $T = 50$ K and $T = 3.2$ K. A gapped magnetic excitation spectrum is clearly visible in the low-temperature data. The data to the left of the black dashed line in (b) was collected using a single orientation for the HYSPEC detector bank. (c) Color contour plot for the alternating chain model described in the text with best fit parameters $J = 3.43(7)$ meV and $J' = 2.25(9)$ meV. The INS data was only fit over the Q - $\hbar\omega$ region presented in this figure.

scattering between 1.5 and 5 meV energy transfer, $\hbar\omega$, with intensity that decreases rapidly as a function of the wavevector transfer, Q . The intensity of this excitation displays a distinct, oscillatory Q -dependence. Both, the temperature and wavevector dependence of this mode, are hallmarks of magnetic fluctuations arising from excited triplet states in a dimerized magnet. No magnetic excitations of higher energy are observed, when neutrons of $E_i = 15$ meV incident energy are used to obtain the data (not shown).

With the magnetic origin of the spectrum established, we next performed an analysis of the INS data using the powder-averaged first frequency moment $\langle E(Q) \rangle$ approach. More specifically, we turn to the following equation, valid for an isotropic spin system with Heisenberg exchange interactions^{20,28,29}:

$$\langle E(Q) \rangle \propto -\sum J_j \langle S_0 \cdot S_{d_j} \rangle |f(Q)|^2 \left(1 - \frac{\sin Qd_j}{Qd_j} \right) \quad (1)$$

where $f(Q)$ is the magnetic form factor for V^{4+} , J_j is the exchange interaction between magnetic ions with spin S separated by a distance d_j , and $\langle S_0 \cdot S_{d_j} \rangle$ is the two-spin correlation function for this pair. The integration ranges used to extract the first frequency moment from the $E_i = 7.5$ and 15 meV measurements were set to 1.5 - 5 meV and 1.25 - 5 meV, respectively, and the data is shown in Fig. 3. Both measurements have an oscillatory intensity that decreases as Q increases. The two datasets were simultaneously fit to Eq. (1) considering only a single value $d_j = d$, but with a multiplicative prefactor and a constant background unique to each value of incident energy. The results of this comparison are shown as solid curves in Fig. 4 revealing excellent agreement for a distance $d = 5.63(4)$ Å. This value is closer and within error of the type-i chain distance compared to the type-ii chain intra-dimer distance. If we fix the value of d in the comparison, we find that the reduced χ^2 value is less for the type-i chain distance ($\chi^2 = 6.675$) compared to the value for the type-ii chain distance ($\chi^2 = 8.602$). We therefore conclude that only along structural chain i magnetic coupling is mediated and not along ii.

Our INS results agrees well with a previous theoretical study assigning the alternating spin chain model based on band structure calculations²⁴ to AgVOAsO_4 with leading J and J' along the structural chain i in the crystal structure. We wish to emphasize that, despite their different directions, the alternating spin chains in AgVOAsO_4 feature same exchange couplings and same spin gap. This is different from the ambient-pressure polymorph of $(\text{VO})_2\text{P}_2\text{O}_7$ ³⁰, where two distinct spin gaps arise from two types of spin chains with dissimilar exchange couplings.

We proceeded to calculate the dynamical structure factor $S(Q, \omega)$ for AgVOAsO_4 using the expression for the alternating Heisenberg spin chain model:

$$S(\vec{Q}, \omega) = A |f(Q)|^2 [1 - \cos(\vec{Q} \cdot \vec{d})] \delta[\hbar\omega - \hbar\omega(\vec{Q})] \quad (2)$$

where A is a multiplicative prefactor and \vec{d} is the vector between spins of the dimer pair with distance d_i . The first order approximation to the alternating chain model dispersion

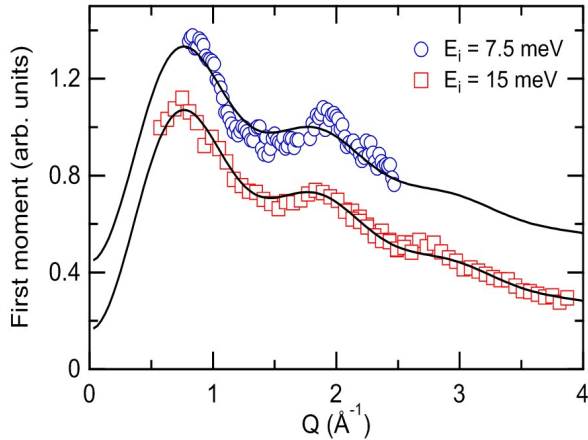


FIG. 3. The powder-averaged first frequency moment as a function of wavevector transfer for both incident energies used in the HYSPEC measurement. An overall normalization factor has been applied so the two datasets can be plotted with the same y-axis. The solid curves represent a simultaneous fit of the data to the first frequency moment expression described in the text with a single exchange interaction.

$\hbar\omega(\vec{Q})$ is given by:

$$\hbar\omega(\vec{Q}) = J - \frac{J'}{2} \cos(\vec{Q} \cdot \vec{u}_0) \quad (3)$$

where J and J' are the exchange interactions of the alternating chain and \vec{u}_0 is the vector connecting the centers of two adjacent dimers. Prior bulk characterization measurements have established that $\alpha = J'/J \approx 0.65$ for AgVOAsO_4 . This larger value of α places the potential dispersion for AgVOAsO_4 far from the first order approximation for the alternating chain model, so we used a modified version of Eq. (3) in our modeling with terms up to third order in α as described in Refs.³¹ and³². To facilitate a direct comparison with our INS data, we powder-averaged Eq. (2) according to the following:

$$S(Q, \omega) = \int \frac{d\Omega_Q}{4\pi} S(\vec{Q}, \omega) \quad (4)$$

More specifically, we calculate $S(\vec{Q}, \omega)$ over spherical shells in Q space at fixed values of energy transfer with \vec{d} and \vec{u}_0 set to the 20 K crystal structure values²⁴ for the proposed magnetic type-i alternating chains. We account for the different chain directions in adjacent ab -planes by including equal contributions from both crystallographic $[1\bar{1}0]$ and $[110]$ directions in our model. The modified spectrum was then multiplied by the appropriate

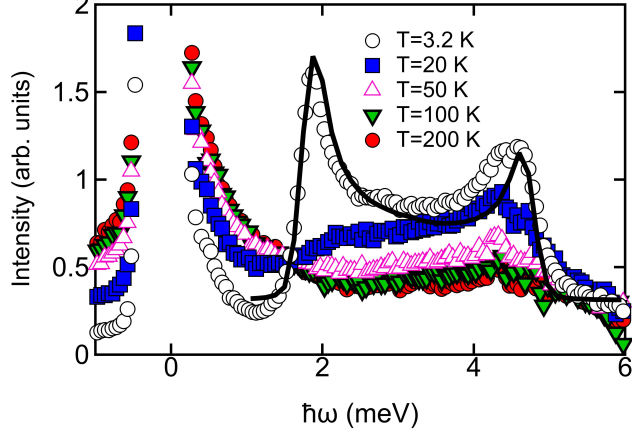


FIG. 4. Temperature-dependence of a constant- Q cut with an integration range $Q = [0.35, 2] \text{ \AA}^{-1}$ from the $E_i = 7.5 \text{ meV}$ HYSPEC dataset. The solid curve superimposed on the 3.2 K data represents a constant- Q cut taken from the best fit simulation shown in Fig. 2(c).

magnetic form factor, $|f(Q)|^2$, for the vanadium ions and convolved with a Gaussian approximation for the instrumental energy and wavevector resolution. A constant background and the multiplicative prefactor were incorporated as fitting parameters of the calculated spectrum in comparison to the measured data. This modeling can accurately reproduce the wavevector and energy-dependence of the measurement when $J = 3.43(7) \text{ meV}$ ($39.8(7)\text{K}$) and $J' = 2.25(9) \text{ meV}$ ($26.2(1)\text{K}$), as shown in Fig. 2(c). The determined exchange interactions and their ratio $\alpha = J'/J = 0.66(3)$ are in excellent agreement with values determined in previous work^{24,27}.

Figure 4 shows constant- Q cuts (integration range $Q = [0.35, 2] \text{ \AA}^{-1}$) for the $E_i = 7.5 \text{ meV}$ data at different temperatures. We superimpose a cut through our model in the figure and find a good overall agreement with the data, however, the measured scattering intensity is not fully-captured near the top of the band between 3 and 5 meV. A large portion of this extra intensity persists up to high temperatures. These combined findings are consistent with a small phonon contribution to the measured spectrum that we do not account for in our modeling. On the other hand, this excess scattering may also arise from two-triplon excitations. This scenario is particularly plausible for quantum paramagnets like AgVOAsO_4 where the triplet excitation bandwidth is much larger than the spin gap, as the continuum of two-triplon modes will then extend down into the single-particle regime³³ that we have modeled above. Single crystal INS data will ultimately be required to definitively establish the origin

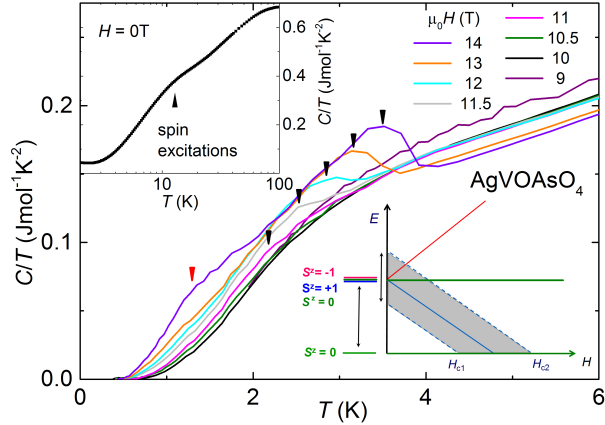


FIG. 5. Specific heat divided by temperature $C(T)/T$ vs T for magnetic fields between 9 T and 14 T with nuclear Schottky contributions subtracted. The measurement at 11 T is the first curve that develops a broad maximum at ~ 2.2 K that becomes more pronounced and shifts to higher T in stronger fields (marked with black arrows). Additionally, a second anomaly appears at ~ 1 K in the 14 T measurement, as indicated by the red arrow. The upper inset shows $C(T)/T$ in zero magnetic field, with a broad hump around 13 K arising from the thermal population of the triplet state. The lower inset displays the energy level scheme for a spin dimer system with both intradimer and interdimer exchange coupling under the application of an external magnetic field.

of the additional scattering in the magnetic excitation spectrum of AgVOAsO_4 .

B. Specific heat

With the alternating chain character confirmed by INS measurements, we now examine the magnetic field and temperature-dependent phase diagram of AgVOAsO_4 . The small spin gap should be closed at an experimentally-accessible critical field H_{c1} and this allows one to search for field-induced magnetic order. We performed specific heat $C(T)$ measurements using a standard relaxation technique in a Quantum Design Physical Property Measurement System with magnetic fields up to 14T. The upper inset in Fig. 5 shows the specific heat divided by temperature $C(T)/T$ in zero field, with a broad hump occurring at 13 K as expected for an interacting, alternating spin chain system with a non-magnetic singlet ground state. We put considerable effort into the preparation of a non-magnetic reference compound to subtract the phonon contribution, however, the non-magnetic analog AgTiOAsO_4 does

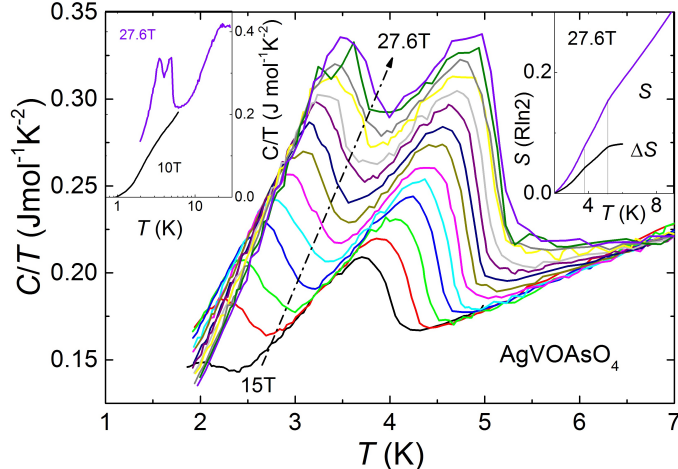


FIG. 6. Specific heat divided by temperature $C(T)/T$ vs T for magnetic fields between 15 T and 27.6 T. Two distinct maxima are observed that move to higher temperatures with increasing field and represent clear evidence for multiple field-induced phase transitions below the onset of the saturated paramagnetic phase at H_{c2} . The left inset displays $C(T)/T$ for the 10 T and maximum field 27.6 T measurements. The right inset shows the calculated entropy $S = \int C(T)/T dT$ in units $R \ln 2$ for the 27.6 T measurement with (i.e. ΔS) and without (i.e. S) subtraction of the 10 T $C(T)/T$ data.

not exist or at least cannot be synthesized under standard conditions.

The specific heat divided by temperature $C(T)/T$ vs T for magnetic fields between 9 - 14 T, with appropriate nuclear Schottky contributions subtracted (discussion below), is shown in Fig. 5. We observe the onset of a broad maximum at 2.2 K in the 11 T data (indicated by a black arrow), in addition to the hump observed at 13K. This anomaly becomes more pronounced in magnetic fields ≥ 11.5 T and provides the first evidence for field-induced magnetic order in this material. A close look at the data obtained at 14 T reveals that the first maximum has shifted to 3.7 K and a second feature in the data is now visible at 1 K, as indicated by the red arrow in Fig. 5.

To map out a larger region of the $H - T$ phase diagram, we extended our measurements to 27.6 T. Specific heat to 27T in a resistive magnet at the Laboratoire National des Champs Magnetiques Intenses in Grenoble, France, using a relaxation dual slope technique³⁴. The data is shown in Fig. 6. We observe that both maxima in $C/T(T)$ develop into distinct λ -anomalies for $H > 15$ T that are typical for second order phase transitions. As mentioned

before, specific heat measurements in high magnetic fields often show a significant nuclear Schottky contribution $[C(T)/T]_{ns}$ at low T caused by isotopes with non-zero nuclear spin. In AgVOAsO_4 , ^{107}Ag and ^{109}Ag ($I = 1/2$, 50% natural abundance each), ^{51}V ($7/2$, 99%), and ^{75}As ($3/2$, 100%) contribute to this effect. As mentioned before, we subtract a contribution of the form $[C(T)/T]_{ns} = a_0 T^{-3}$ from the data shown in Fig. 5. The estimated prefactor $a_0 = 1.55$ mJ-K/mol in low fields increases by 30% for the 14 T measurement. Enlarged a_0 values above H_{c1} are a further indication for field-induced order, since the internal magnetic field detected by the nuclear spins is strongly enhanced.

The full entropy of a spin-1/2 dimer system is $R \ln 2$, which is released when the thermal energy is significantly larger than the intradimer exchange J^{35} . Since our INS measurements find the primary exchange constant to be approximately $J = 40$ K, we expect the high- T entropy regime to onset well above the 13 K maximum observed in the zero-field specific heat data. In the left inset of Fig. 6, we show $C(T)/T$ for the 10 T and 27.6 T measurements on the same scale to facilitate an easier comparison. The right inset shows the calculated entropy for the 27.6 T measurement with (i.e. ΔS) and without (i.e. S) subtraction of the specific heat measured in 10T. About 30% of the maximum entropy $R \ln 2$ is recovered upon warming up to 10 K with only a few percent released at each of the two phase transitions. As shown later, these small differences in entropy are sufficiently large to track the phase boundaries in magnetocaloric effect (MCE) measurements under quasiadiabatic conditions.

C. Magnetization

We continue our high-field study with magnetization measurements. Extraction magnetometry has been utilized to measure $M(H)$ between 0.5K and 10K up to 60T inside a capacitor-driven pulsed magnet at the Pulsed Field Facility of the National High Magnetic Field Laboratory (NHMFL). Signatures in $M(H)$ have been used successfully in the past to estimate the phase diagram of related compounds³⁶. Fig. 7 shows the magnetization of AgVOAsO_4 measured up to 60 T with the initial sample temperature $T_0(H = 0)$ in the range between 0.56 K and 10 K. At low T , we can distinguish three different field regions. In fields up to 5 T, the magnetization is dominated by the paramagnetic behavior of unpaired spins arising from defects in the crystal structure²⁷. Above 5 T these unpaired spins are fully-polarized, which leads to a constant background in the quantum paramagnetic state.

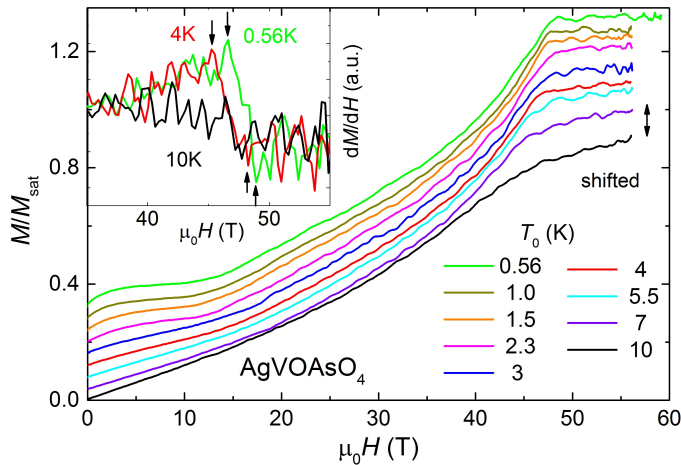


FIG. 7. Magnetization $M(H)$ vs magnetic field H measured in high fields to 60 T is shown for initial temperatures T_0 between 0.56 K and 10 K (data are offset vertically for better visibility). The inset shows dM/dH close to H_{c2} for the measurements at 0.56 K and 4 K with a clear maximum followed by a step down indicating a double phase transition. In contrast, a more smooth behavior in dM/dH is observed at 10K.

Starting at a critical field H_{c1} near 10 T, the magnetization increases monotonically and reaches saturation at about 48 T. The field-dependence of $M(H)$ can be reproduced with an interacting, alternating spin chain model²⁴. The magnetization close to full saturation reveals two distinct changes in the slope at $\mu_0 H_{c2'} = 46.6$ T and $\mu_0 H_{c2} = 48.8$ T, as can be seen more clearly in the derivative $\partial M/\partial H$ in the inset of Fig 7.

In order to identify multiple phase transitions in magnetization measurements close to the lower critical field H_{c1} , we extend our experiments down to 0.1K temperature. This approach is necessary because quantum fluctuations significantly alter thermodynamic signatures of second order phase transitions at the onset of field-polarization in quantum magnets. The effect depends on the renormalized mass m^* of the bosons, which scales with the ratio of the critical fields: $m^* \propto H_{c1}/H_{c2}$ at H_{c1} ³⁷. Notably, mass renormalization does not occur close to H_{c2} , because here the fully polarized system behaves classically. Therefore, asymmetric thermodynamic anomalies (i.e. sharper near H_{c2} versus near H_{c1}) are expected in AgVOAsO₄. Fig. 8 shows $M(H)$ vs H for magnetic fields between 7.4 T and 12 T. A dilution refrigerator equipped with a 12 T superconducting magnet and a Faraday magnetometer was used to obtain $M(H)$ and $M(T)$ down to 0.1 K close to the critical fields H_{c1} and H'_{c1} . We observe two slope changes in $M(H)$, corresponding to two weakly- T dependent

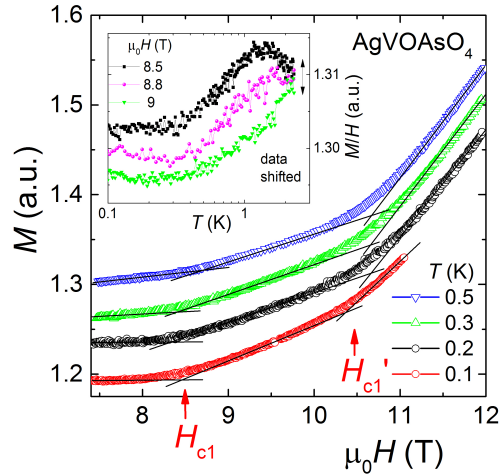


FIG. 8. Magnetization $M(H)$ versus magnetic field H in the field range 7.4 T to 12 T for T between 0.1 K and 0.5 K. The measurements are offset from one another to ensure better visibility. We observe two changes of slope in $M(H)$ at $\mu_0 H_{c1} = 8.4$ T and $\mu_0 H_{c1'} = 10.5$ T, which identify two field-induced phase transitions. The inset shows $M(T)/H$ vs T collected in fields of 8.5 T, 8.8 T and 9 T. A broad maximum is observed in this data that is used to define the H_{c1} phase boundary.

phase transitions, at $\mu_0 H_{c1} = 8.4$ T and at $\mu_0 H_{c1'} = 10.5$ T. We also carried out T -dependent $M(T)$ measurements in constant magnetic fields between 7 T and 12 T, and we find a very small T -dependence in the data as expected from the light boson mass. A maximum in $M(T)$ is observed at the lower $H_{c1}(T)$ phase boundary, as seen in the inset of Fig. 8, that moves to higher T with increasing field, but no clear signature in $M(T)$ is resolved close to the $H_{c1'}(T)$ phase boundary line.

D. Phase diagram and MCE

Fig. 9 summarizes the phase transitions obtained by specific heat and magnetization measurements in pulsed and static magnetic fields. These measurements map out a double-dome phase diagram with $\mu_0 H_{c1} = 8.4$ T, $\mu_0 H_{c1'} = 10.5$ T, $\mu_0 H_{c2'} = 46.6$ T and $\mu_0 H_{c2} = 48.9$ T. We complete our investigations of the high-field properties in AgVOAsO₄ with MCE measurements carried out in a capacitor-driven pulsed magnet (pulse duration 36ms) at the International MegaGauss Science Laboratory of the University of Tokyo. In the experiment, the sample is kept under quasi-adiabatic conditions during fast changing field pulses and

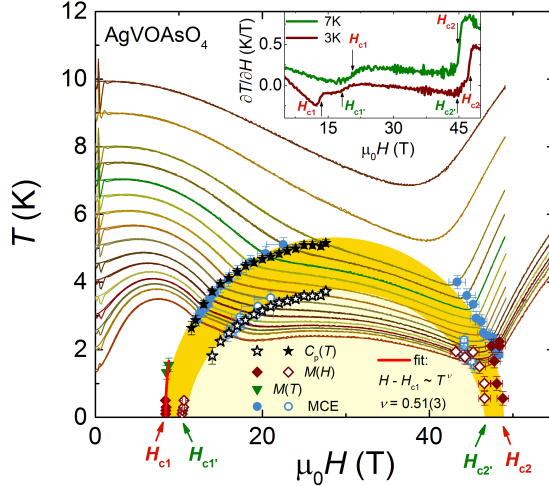


FIG. 9. $H - T$ phase diagram of AgVOAsO_4 obtained from specific heat, MCE, and magnetization experiments. We observe clear signatures of two different field-induced ordered states. Lines of constant entropy obtained under adiabatic conditions in pulsed fields illustrate the MCE and confirm the double dome structure of the phase diagram. A power law fit $H - H_{c1} \propto T^\nu$ of the phase boundary at H_{c1} reveals 0.51(3) as the critical exponent. The inset shows the derivative $\partial T/\partial H$ for MCE measurements with zero field temperatures $T_0 = 3$ K and 7 K. Arrows mark the critical fields H_{c1} , $H_{c1'}$, $H_{c2'}$ and H_{c2} .

the sample temperature is monitored, which yields isentropic temperature lines as included in Fig. 9. The polarization of free spins up to 5 T is reflected in a smooth increase of the temperature because the entropy decreases gradually. A careful analysis of the derivative $\partial T/\partial H$, shown for the $T_0 = 3$ K and $T_0 = 7$ K measurements in the inset of Fig. 9, reveals four clear steps corresponding to the crossing points of the four phase transitions in the 3K data, whereas only two steps are resolved in the 7K measurement. These results are consistent with the phase lines extracted from specific heat and magnetization measurements. Furthermore, the MCE isentropes exhibit a clear asymmetric behavior with a shallow minimum in $T(H)$ close to H_{c1} indicating a (relative) small entropy accumulation and a deeper minimum around H_{c2} indicating more accumulated entropy. This effect can be explained again with a renormalized boson mass close to H_{c1} and a bare boson mass close to H_{c2} . Moreover, the MCE measurements allow us to refine the actual sample temperature in the magnetization experiments when crossing through the phase boundaries, because the magnetization and MCE measurements were collected under similar thermodynamic conditions

in pulsed magnetic fields.

III. DISCUSSION

We want to emphasize that a clear double anomaly observed in both the low and high field regimes of the $H - T$ phase diagram for AgVOAsO_4 cannot be explained by magnetic anisotropy. For a polycrystalline, anisotropic sample, only one broad anomaly in $C(T)/T$ is expected because all grains are randomly-oriented and therefore should contribute equally to the anomaly through a continuous spectrum of critical fields. Also, we found no evidence for anisotropy-induced splitting of the triplet excitation in our INS measurements. We furthermore can rule out antisymmetric exchange interactions based on symmetry considerations. AgVOAsO_4 belongs to the space group $P2_1/c$ that features inversion centers between the vanadium atoms²⁴. Finally, ESR measurements reveal a nearly isotropic g-factor²⁴, with $g_{\parallel} = 1.92$ and $g_{\perp} = 1.96$. The 2% g-factor anisotropy is equivalent to a 0.2 T difference in the critical fields $\mu_0|H_{c1} - H_{c1'}|$ and less than a 1 T difference $\mu_0|H_{c2} - H_{c2'}|$. These values are much smaller than the 2 T difference in the critical fields that we have identified here on both the low and high field sides of the phase diagram.

As mentioned before, both phase transitions can be classified as second order, because i) the anomaly in $C(T)/T$ shows the typical λ -shape, ii) no hysteresis or dissipative behavior is observed in the measurements, and iii) we observe asymmetry in the thermodynamic anomalies measured at H_{c1} and H_{c2} , which are caused by quantum fluctuations only present at 2^{nd} order transitions. Subsequently, we analyze the critical behavior of the phase boundary up to 1.55 K (Fig. 9) with a power law $T \propto |H - H_{c1}|^{\nu}$ using $\mu_0 H_{c1} = 8.4$ T and we obtain $\nu = 0.51 \pm 0.13$. This value corroborates the 3D BEC scenario ($\nu = 2/3$)⁴.

Theoretical work based on density matrix renormalization group (DMRG) calculations for $\alpha = 0.45$ in the alternating chain model finds a complex $H - T$ phase diagram with a phase of incommensurate magnetic order terminated by a first order transition inside a larger dome of a commensurate one³⁸⁻⁴⁰. The asymmetric inner dome appears when intra-chain next-nearest neighbor frustration exceeds 10% of nearest-neighbor coupling, which is equivalent to bond frustration connecting the *same dimers in the same chain*⁴. We want to stress that AgVOAsO_4 represents the case of frustrated exchange interactions connecting alternating chains and therefore *different dimers* in different ab -planes²⁴. Only for the later

case, a multi- \mathbf{Q} BEC is expected with coexistence of XY-AFM and Ising-like ordering in the very same phase. The magnetic isotropy of the V^{4+} moments, the symmetry of the phase diagram, the frustrated interdimer interactions, as well as the second order phase boundaries found for AgVOAsO_4 point to the possibility to find multi- $\vec{\mathbf{Q}}$ BEC in this material.

IV. SUMMARY

In summary, we have used inelastic neutron scattering experiments on polycrystalline samples of the quantum paramagnet AgVOAsO_4 to confirm that this system is well described by an alternating spin chain model. We have established the $H - T$ phase diagram for AgVOAsO_4 with specific heat, MCE and magnetization measurements in high magnetic fields and down to low temperatures. We find evidence for a symmetric double-dome phase diagram with field-induced order between $\mu_0 H_{c1} = 8.4$ T and $\mu_0 H_{c2} = 48.9$ T. This complex phase diagram establishes AgVOAsO_4 as a promising multi- $\vec{\mathbf{Q}}$ BEC candidate capable of hosting exotic topological spin structures. Future NMR or neutron diffraction measurements on single crystals above the lower critical fields H_{c1} and $H_{c1'}$ are essential for elucidating the microscopic spin arrangements of the two field-induced ordered phases in this material.

V. ACKNOWLEDGMENTS

F.W. thanks Cristian D. Batista for fruitful discussions. A portion of this research used resources at the Spallation Neutron Source, a DOE Office of Science User Facility operated by Oak Ridge National Laboratory (ORNL). The National High Magnetic Field Laboratory is supported by the National Science Foundation Cooperative Agreement No. DMR-1157490, the State of Florida and the United States Department of Energy. N.H. acknowledges support from the DOE BES project: Science in 100 Tesla.

* weickert@lanl.gov

† aczelaa@ornl.gov

¹ Y. Kamiya and C. D. Batista, Phys. Rev. X **4**, 011023 (2014).

- ² S. Mühlbauer, B. Binz, F. Jonietz, C. Pfleiderer, A. Rosch, A. Neubauer, R. Georgii, and P. Böni, *Science* **323**, 915 (2009).
- ³ S. Seki, X. Z. Yu, S. Ishiwata, and Y. Tokura, *Science* **336**, 198 (2012).
- ⁴ V. Zapf, M. Jaime, and C. D. Batista, *Rev. Mod. Phys.* **86**, 563 (2014).
- ⁵ T. Nikuni, M. Oshikawa, A. Oosawa, and H. Tanaka, *Phys. Rev. Lett.* **84**, 5868 (2000).
- ⁶ M. Jaime, V. F. Correa, N. Harrison, C. D. Batista, N. Kawashima, Y. Kazuma, G. A. Jorge, R. Stern, I. Heinmaa, S. A. Zvyagin, Y. Sasago, and K. Uchinokura, *Phys. Rev. Lett.* **93**, 087203 (2004).
- ⁷ V. S. Zapf, D. Zocco, B. R. Hansen, M. Jaime, N. Harrison, C. D. Batista, M. Kenzelmann, C. Niedermayer, A. Lacerda, and A. Paduan-Filho, *Phys. Rev. Lett.* **96**, 077204 (2006).
- ⁸ V. O. Garlea, A. Zheludev, T. Masuda, H. Manaka, L.-P. Regnault, E. Ressouche, B. Grenier, J.-H. Chung, Y. Qiu, K. Habicht, K. Kiefer, and M. Boehm, *Phys. Rev. Lett.* **98**, 167202 (2007).
- ⁹ E. C. Samulon, Y.-J. Jo, P. Sengupta, C. D. Batista, M. Jaime, L. Balicas, and I. R. Fisher, *Phys. Rev. B* **77**, 214441 (2008).
- ¹⁰ A. A. Aczel, Y. Kohama, M. Jaime, K. Ninios, H. B. Chan, L. Balicas, H. A. Dabkowska, and G. M. Luke, *Phys. Rev. B* **79**, 100409(R) (2009).
- ¹¹ A. A. Aczel, Y. Kohama, C. Marcenat, F. Weickert, M. Jaime, O. Ayala-Valenzuela, R. D. McDonald, S. D. Selesnic, H. A. Dabkowska, and G. M. Luke, *Phys. Rev. Lett.* **103**, 207203 (2009).
- ¹² H. Yamaguchi, H. Miyagai, M. Yoshida, M. Takigawa, K. Iwase, T. Ono, N. Kase, K. Araki, S. Kittaka, T. Sakakibara, T. Shimokawa, T. Okubo, K. Okunishi, A. Matsuo, and Y. Hosokoshi, *Phys. Rev. B* **89**, 220402 (2014).
- ¹³ Y. Kono, H. Yamaguchi, Y. Hosokoshi, and T. Sakakibara, *Phys. Rev. B* **96**, 104439 (2017).
- ¹⁴ T. Matsubara and H. Matsuda, *Progress of Theoretical Physics* **16**, 569 (1956).
- ¹⁵ E. Batyev and L. Braginskii, *Sov. Phys. JETP* **60**, 781 (1984).
- ¹⁶ I. Affleck, *Phys. Rev. B* **43**, 3215 (1991).
- ¹⁷ T. Giamarchi and A. M. Tsvelik, *Phys. Rev. B* **59**, 11398 (1999).
- ¹⁸ T. Giamarchi, C. Rüegg, and O. Tchernyshyov, *Nature Physics* **4**, 198 (2008).
- ¹⁹ M. B. Stone, M. D. Lumsden, S. Chang, E. C. Samulon, C. D. Batista, and I. R. Fisher, *Phys. Rev. Lett.* **100**, 237201 (2008).

- ²⁰ M. B. Stone, M. D. Lumsden, Y. Qiu, E. C. Samulon, C. D. Batista, and I. R. Fisher, *Phys. Rev. B* **77**, 134406 (2008).
- ²¹ E. C. Samulon, K. A. Al-Hassanieh, Y.-J. Jo, M. C. Shapiro, L. Balicas, C. D. Batista, and I. R. Fisher, *Phys. Rev. B* **81**, 104421 (2010).
- ²² M. B. Stone, M. D. Lumsden, V. O. Garlea, B. Grenier, E. Ressouche, E. C. Samulon, and I. R. Fisher, *Phys. Rev. B* **92**, 020415 (2015).
- ²³ S. Suh, K. A. Al-Hassanieh, E. C. Samulon, I. R. Fisher, S. E. Brown, and C. D. Batista, *Phys. Rev. B* **84**, 054413 (2011).
- ²⁴ A. A. Tsirlin, R. Nath, J. Sichelschmidt, Y. Skourski, C. Geibel, and H. Rosner, *Phys. Rev. B* **83**, 144412 (2011).
- ²⁵ G. Xu, C. Broholm, D. H. Reich, and A. M. A., *Phys. Rev. Lett.* **84**, 4465 (2000).
- ²⁶ M. B. Stone, Y. Chen, D. H. Reich, C. Broholm, G. Xu, J. R. D. Copley, and J. C. Cook, *Phys. Rev. B* **90**, 094419 (2014).
- ²⁷ N. Ahmed, P. Khuntia, K. M. Ranjith, H. Rosner, M. Baenitz, A. A. Tsirlin, and R. Nath, *Phys. Rev. B* **96**, 224423 (2017).
- ²⁸ P. C. Hohenberg and W. F. Brinkman, *Phys. Rev. B* **10**, 128 (1974).
- ²⁹ C. Tassel, J. Kang, C. Lee, O. Hernandez, Y. Qiu, W. Paulus, E. Collet, B. Lake, T. Guidi, M.-H. Whangbo, C. Ritter, H. Kageyama, and S.-H. Lee, *Phys. Rev. Lett.* **105**, 167205 (2010).
- ³⁰ T. Yamauchi, Y. Narumi, J. Kikuchi, Y. Ueda, K. Tatani, T. C. Kobayashi, K. Kindo, and K. Motoya, *Phys. Rev. Lett.* **83**, 3729 (1999).
- ³¹ A. Brooks Harris, *Phys. Rev. B* **7**, 3166 (1973).
- ³² T. Barnes, J. Riera, and D. A. Tennant, *Phys. Rev. B* **59**, 11384 (1999).
- ³³ M. B. Stone, I. A. Zaliznyak, T. Hong, C. L. Broholm, and D. H. Reich, *Nature* **440**, 187 (2006).
- ³⁴ S. Riegel and G. Weber, *Journal of Physics E: Scientific Instruments* **19**, 790 (1986).
- ³⁵ J. Brambleby, P. A. Goddard, J. Singleton, M. Jaime, T. Lancaster, L. Huang, J. Wosnitza, C. V. Topping, K. E. Carreiro, H. E. Tran, Z. E. Manson, and J. L. Manson, *Phys. Rev. B* **95**, 024404 (2017).
- ³⁶ S. E. Sebastian, N. Harrison, C. Batista, L. Balicas, M. Jaime, P. Sharma, N. Kawashima, and I. Fisher, *Journal of Magnetism and Magnetic Materials* **310**, e460 (2007).

- ³⁷ Y. Kohama, A. V. Sologubenko, N. R. Dilley, V. S. Zapf, M. Jaime, J. A. Mydosh, A. Paduan-Filho, K. A. Al-Hassanieh, P. Sengupta, S. Gangadharaiah, A. L. Chernyshev, and C. D. Batista, *Phys. Rev. Lett.* **106**, 037203 (2011).
- ³⁸ N. Maeshima, K. Okunishi, K. Okamoto, and T. Sakai, *Phys. Rev. Lett.* **93**, 127203 (2004).
- ³⁹ N. Maeshima, K. Okunishi, K. Okamoto, T. Sakai, and K. Yonemitsu, *J. Phys. Soc. Jpn.* **74**, 63 (2005).
- ⁴⁰ N. Maeshima, K. Okunishi, K. Okamoto, T. Sakai, and K. Yonemitsu, *J. Phys.: Cond. Matt.* **18**, 4819 (2006).